Grazing bifurcation analysis of a relative rotation system with backlash non-smooth characteristic*

Liu Shuang(刘 爽)[a)b)], Wang Zhao-Long(王兆龙)[a)†], Zhao Shuang-Shuang(赵双双)[a)], Li Hai-Bin(李海滨)[a)b)], and Li Jian-Xiong(李建雄)[a)b)]

[a)] *Key Laboratory of Industrial Computer Control Engineering of Hebei Province, Yanshan University, Qinhuangdao* 066004, *China*
[b)] *National Engineering Research Center for Equipment and Technology of Cold Strip Rolling, Yanshan University, Qinhuangdao* 066004, *China*

(Received 5 December 2014; revised manuscript received 7 January 2015; published online 29 May 2015)

Grazing bifurcation of a relative rotation system with backlash non-smooth characteristic is studied along with the change of the external excitation in this paper. Considering the oil film, backlash, time-varying stiffness and time-varying error, the dynamical equation of a relative rotation system with a backlash non-smooth characteristic is deduced by applying the elastic hydrodynamic lubrication (EHL) and the Grubin theories. In the process of relative rotation, the occurrence of backlash will lead to the change of dynamic behaviors of the system, and the system will transform from the meshing state to the impact state. Thus, the zero-time discontinuous mapping (ZDM) and the Poincare mapping are deduced to analyze the local dynamic characteristics of the system before as well as after the moment that the backlash appears (i.e., the grazing state). Meanwhile, the grazing bifurcation mechanism is analyzed theoretically by applying the impact and Floquet theories. Numerical simulations are also given, which confirm the analytical results.

Keywords: relative rotation system, backlash, grazing bifurcation, zero-time discontinuous mapping

PACS: 45.20.dc, 05.45.–a **DOI:** 10.1088/1674-1056/24/7/074501

1. Introduction

The relative rotation system, as a widespread energy transmission system in the project, has drawn much attention in recent years. Luo set up the theory of relativistic analytical mechanics of the rotational systems in 1996,[1–3] which was applied to the research on the symmetry theory of dynamical systems.[4–6] Various nonlinear factors are contained in the relative rotation system, which lead to the system to produce complex dynamic behaviors such as bifurcation and chaos. Bifurcation and chaos are important parts of the nonlinear scientific fields.[7–10] They have achieved rapid development and extensive applications in the fields of secure communications[11–13] and signal processing.[14–16] At the same time, the Hopf bifurcation was analyzed on the basis of the relative rotation theory, and the nonlinear and nonlinear time-delayed feedback control techniques were proposed to control the bifurcation points and the stability of periodic solutions.[17–19] The bifurcation response equation of the relative rotation system was deduced with the method of multiple scales, and the bifurcation and chaotic motions under combination resonance were investigated.[20,21] The parameter stability and global bifurcations of a strong nonlinear system with parametric excitations and external excitations were investigated using the method of multiple scales.[22] The existence of both Hopf bifurcation and the topological horseshoe for a novel finance chaotic system was investigated.[23] The anti vibratory passive and active methods were applied to complex mechanical systems.[24] The nonlinear free vibrations of the electromechanical integrated toroidal drive system were investigated using the perturbation method.[25] However, all the systems studied in the above-mentioned literatures are smooth dynamical systems, in which the nonsmooth factors are neglected. In addition, some nonsmooth factors may lead to grazing bifurcation and induce the oscillatory instability.

Grazing bifurcation is a proprietary bifurcation in the nonsmooth dynamical system. The sliding and grazing bifurcations in periodically forced oscillators with dry friction were extensively investigated.[26–28] A linear oscillator undergoing impacts with a secondary elastic support was studied, and both smooth and nonsmooth bifurcations were observed.[29] An impacting system was investigated, the results of which showed that the periodic windows in the locus of boundary crises were caused by grazing bifurcations intersecting the locus of boundary crises and that grazing bifurcations can affect the existence of the boundary saddle-point solutions.[30,31] The existence and stability of the grazing periodic trajectory in a two-degree-of-freedom vibro-impact system were investigated.[32] The relationship between the saddle-node and grazing bifurcations in periodically-forced impact oscillators was investigated.[33] The complex oscillations caused by the occurrence of grazing bifurcations in a pressure relief valve were investigated.[34] A non-smooth model of a Jeffcott rotor was investigated. The study revealed a rich variety of dynam-

*Project supported by the National Natural Science Foundation of China (Grant No. 61104040), the Natural Science Foundation of Hebei Province, China (Grant No. E2012203090), and the University Innovation Team of Hebei Province Leading Talent Cultivation Project, China (Grant No. LJRC013).

†Corresponding author. E-mail: zlwang1988@163.com

© 2015 Chinese Physical Society and IOP Publishing Ltd

ics, which included grazing-induced fold and period-doubling bifurcations.[35] However, the systems in the above-mentioned literatures are linear and impact systems, some of which were studied directly by numerical simulations. Up to now, there have only been a few researches about grazing bifurcations for nonlinear systems with nonsmooth properties from the perspective of theory and mechanism.

In this paper, considering the nonsmooth and nonlinear characteristics, the dynamical equation of a nonlinear relative rotation system with backlash non-smooth characteristic is deduced. The grazing bifurcation mechanism is theoretically analyzed. Numerical simulations are also given, which confirm the analytical results and show that the grazing bifurcation can lead to the chaotic motion. Moreover, the research in this paper provides a theoretical reference for the design and control of the transmission system in practical engineering.

The rest of the paper is organized as follows. The dynamic model of the nonsmooth relative rotation system with backlash is presented in Section 2. The grazing bifurcation mechanism is analyzed in Section 3. Numerical simulations are performed in Section 4, and some concluding remarks are provided in Section 5.

2. The dynamic model of the nonsmooth relative rotation system with backlash

Considering the main drive system driven by an electrical motor, the transmissions between the motor and the load are gears. The motor and the drive gear are connected by a rigid shaft, so that they can be equivalent to a concentrated mass. A similar method can be applied to the load and the driven gear. Meanwhile, considering the influence of backlash, time-varying characteristics and oil film, the structure of the two-mass system is shown in Fig. 1.

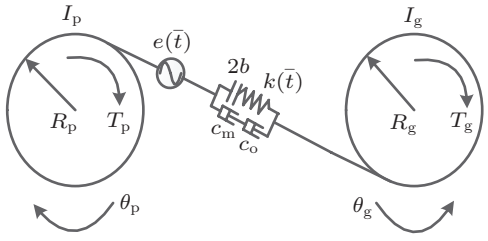


Fig. 1. The dynamic model of nonsmooth relative rotation system with backlash.

The parameters are as follows: I_p and I_g are the rotational inertias of the drive and driven gears, respectively, R_p and R_g are the base radiuses of the drive and driven gears, respectively, T_p and T_g are the input torque and the load torque, respectively, θ_p and θ_g are the vibratory angular displacements of the drive and driven gears, respectively, $2b$ is the total backlash, c_m is the meshing damping coefficient, c_o is the oil film damping coefficient, $k(\bar{t})$ is the time-varying stiffness, and $e(\bar{t})$ is the static transmission error caused by manufacturing. Here,

$$k(\bar{t}) = k_m + k_q \cos(\omega \bar{t} + \pi), \tag{1}$$

where k_m is the mean mesh stiffness, k_q is the variable amplitude of mesh stiffness, ω is the tooth mesh frequency, and

$$e(\bar{t}) = e_a \cos(\omega \bar{t} + \phi_c), \tag{2}$$

where e_a is the variable amplitude of unload static error, ω is the tooth mesh frequency, and ϕ_c is the initial phase.

The width of the backlash is determined by the linear displacement difference between the two gears, so the transmission error of the linear displacement is defined as

$$q = R_p \theta_p - R_g \theta_g - e(\bar{t}). \tag{3}$$

The backlash function is defined as

$$f(q) = \begin{cases} q - b, & q > b, \\ 0, & -b \le q \le b, \\ q + b, & q < -b. \end{cases} \tag{4}$$

As shown in Fig. 1, the internal dynamic force can be expressed as

$$F_d = c_m c_o / (c_m + c_o) q + k(\bar{t}) f(q). \tag{5}$$

According to Newton's law, the dynamical equation of a relative rotation system with backlash nonsmooth characteristic under the oil film force can be expressed as

$$\begin{cases} I_p \ddot{\theta}_p + R_p F_d = T_p, \\ I_g \ddot{\theta}_g - R_g F_d = -T_g. \end{cases} \tag{6}$$

During the actual transmission process, the oil film damping is influenced by many factors. Meanwhile, when the backlash appears between the mating gear teeth, the oil will leak, so the oil film can be ignored. In this paper, the oil film damping is considered only when the mating gear teeth mesh with each other.

Under the conditions that the density and viscosity of the oil film are constant, the Reynolds equation is introduced,[36] which can be used to describe the distribution of pressure between the contact surfaces

$$\frac{\partial}{\partial \bar{\xi}} \left(h^3 \frac{\partial p}{\partial \bar{\xi}} \right) = 12 u \overline{\eta} \frac{\partial h}{\partial \bar{\xi}} + 12 \overline{\eta} \frac{\partial h}{\partial \bar{t}}, \tag{7}$$

where $u = (u_p + u_g)/2$, h is the oil film thickness, $\overline{\eta}$ is the oil film viscosity, p is the oil film pressure, u is the entraining velocity, u_p and u_g are the surface tangential velocities of gear pairs, and $\bar{\xi}$ is the direction of relative rotation.

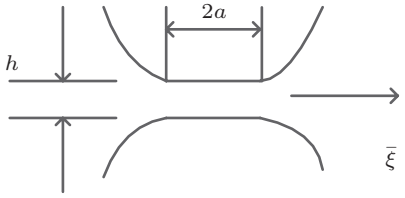


Fig. 2. Grubin contact model.

When the oil film thickness is constant in the contact area, the Grubin theory is introduced.[36] Therefore, the oil film thickness h is constant along the $\overline{\xi}$ direction (Fig. 2), i.e., $\partial h/\overline{\xi} = 0$. In addition,

$$h = 1.95(\alpha\overline{\eta}u)^{8/11}R^{4/11}\left(\frac{E'}{w}\right)^{1/11}, \tag{8}$$

where α is the pressure–viscosity coefficient of oil, R is the equivalent radius, E' is the equivalent elastic modulus, w is the load per unit length, a is the semi-width of the contact area, η_0 is the nominal oil film viscosity, and $a = [8wR/(\pi E')]^{1/2}$. Then, equation (7) reduces to

$$\frac{\partial}{\partial\overline{\xi}}\left(h^3\frac{\partial p}{\partial\overline{\xi}}\right) = 12\overline{\eta}\frac{\partial h}{\partial\overline{t}}. \tag{9}$$

By integrating Eq. (9) with the following boundary conditions:

$$p = 0, \quad \overline{\xi} = \pm a, \quad \frac{\partial p}{\partial\overline{\xi}} = 0, \quad \overline{\xi} = 0, \tag{10}$$

$p(\overline{\xi})$ can be obtained. Then, oil film force $\overline{F}_{\rm o}$ can be obtained by integrating $p(\overline{\xi})$ in the contact area $(-a \le \overline{\xi} \le a)$ as

$$\overline{F}_{\rm o} = -\frac{8a^3\overline{\eta}l}{h^3}\frac{\partial h}{\partial\overline{t}}, \tag{11}$$

where l is the axial length of the contact area, and $\partial h/\partial\overline{t}$ is the squeezing velocity, i.e., $\partial h/\partial\overline{t} = \dot{q}$. The negative sign indicates that the direction of the oil film force is opposite to the squeezing velocity direction of the oil film. If the squeezing velocity is positive, the oil film force is a damping force. Hence,

$$c_{\rm o} = \frac{8a^3\overline{\eta}l}{h^3}. \tag{12}$$

Let $m_{\rm e} = I_{\rm p}I_{\rm g}/(I_{\rm p}R_{\rm g}^2 + I_{\rm g}R_{\rm p}^2)$, $F_{\rm m} = T_{\rm p}/R_{\rm p} = T_{\rm g}/R_{\rm g}$, $F_{\rm q} = m_{\rm e}e_{\rm a}\omega^2$, $t = \omega_{\rm n}\bar{t}$, $\Omega = \omega/\omega_{\rm n}$, ($\omega_{\rm n}$ is the angular natural frequency, $\omega_{\rm n} = \sqrt{k_{\rm m}/m_{\rm e}}$), $y = q/b$, $\phi_{\rm c} = \pi$, $\zeta = c_{\rm m}/2m_{\rm e}\omega_{\rm n}$, $\sigma = k_{\rm q}/k_{\rm m}$, $P_{\rm m} = F_{\rm m}/(m_{\rm e}b\omega_{\rm n}^2)$, $P_{\rm q} = F_{\rm q}/(m_{\rm e}b\omega_{\rm n}^2)$, $H = h/R$, $W = w/(E'R)$, $U = \eta_0 u/(E'R)$, $G = \alpha E'$, $\xi = \overline{\xi}/a$, $P = p/E'$, $\eta = \overline{\eta}/\eta_0$, $L = l/R$, and $A = \eta_0\omega_{\rm n}a^2/(E'R^2)$, then, the dimensionless time-varying stiffness is

$$k(t) = 1 + \sigma\cos(\Omega t + \pi). \tag{13}$$

The dimensionless backlash function is

$$f(y) = \begin{cases} y-1, & y \ge 1, \\ 0, & -1 < y < 1, \\ y+1, & y \le 1. \end{cases} \tag{14}$$

The dimensionless oil film force is

$$F_{\rm o} = -\frac{8A\eta L}{H^3}\frac{\partial H}{\partial t} = -\mu_{\rm o}\dot{y}. \tag{15}$$

The dimensionless oil film damping is $\mu_{\rm o} = c\eta P_{\rm m}^{\frac{14}{11}}/\Omega^{\frac{24}{11}}$, where c is constant. Thus, the dimensionless system model can be expressed as

$$\begin{cases} \ddot{y} + 2\zeta\mu_{\rm o}/(2\zeta+\mu_{\rm o})\dot{y} + k(t)(y-1) = P_{\rm m} + P_{\rm q}\cos(\Omega t+\pi), & y \ge 1, \\ \ddot{y} + 2\zeta\dot{y} = P_{\rm m} + P_{\rm q}\cos(\Omega t+\pi), & -1 < y < 1, \\ \ddot{y} + 2\zeta\mu_{\rm o}/(2\zeta+\mu_{\rm o})\dot{y} + k(t)(y+1) = P_{\rm m} + P_{\rm q}\cos(\Omega t+\pi), & y \le -1, \end{cases} \tag{16}$$

Let $x = y - 1$, and the system model can be rewritten as

$$\begin{cases} \ddot{x} + 2\zeta\mu_{\rm o}/(2\zeta+\mu_{\rm o})\dot{x} + k(t)x = P_{\rm m} + P_{\rm q}\cos(\Omega t+\pi) & x \ge 0, \\ \ddot{x} + 2\zeta\dot{x} = P_{\rm m} + P_{\rm q}\cos(\Omega t+\pi), & -2 < x < 0, \\ \ddot{x} + 2\zeta\mu_{\rm o}/(2\zeta+\mu_{\rm o})\dot{x} + k(t)(x+2) = P_{\rm m} + P_{\rm q}\cos(\Omega t+\pi), & x \le -2. \end{cases} \tag{17}$$

Let $x_1 = x$, $x_2 = \dot{x}$, and $x_3 = \Omega t$, then, the state equation of the system can be expressed as

$$\dot{x} = \begin{cases} F_1, & x \in S_1, \\ F_2, & x \in S_2, \\ F_3, & x \in S_3. \end{cases} \tag{18}$$

The state space is divided into three subspaces

$$S_1 = \left\{x \in R^3 | K(x) > 0\right\},$$
$$S_2 = \left\{x \in R^3 | -2 \le K(x) \le 0\right\},$$
$$S_3 = \left\{x \in R^3 | K(x) < -2\right\},$$

where $x = (x_1, x_2, x_3)^{\rm T}$, $K(x) = x_1$,

$$F_1 = \begin{pmatrix} x_2 \\ -2\zeta\mu_{\rm o}/(2\zeta+\mu_{\rm o})x_2 - (1+\sigma\cos(x_3+\pi))x_1 + P_{\rm m} + P_{\rm q}\cos(x_3+\pi) \\ \Omega \end{pmatrix},$$

$$F_2 = \begin{pmatrix} x_2 \\ -2\zeta x_2 + P_{\rm m} + P_{\rm q}\cos(x_3+\pi) \\ \Omega \end{pmatrix},$$

$$F_3 = \begin{pmatrix} x_2 \\ -2\zeta\mu_o/(2\zeta+\mu_o)x_2 - (1+\sigma\cos(x_3+\pi))(x_1+2) + P_m + P_q\cos(x_3+\pi) \\ \Omega \end{pmatrix}.$$

Equation (18) is the dynamical state equation of the non-smooth relative rotation system considering oil film damping, backlash, time-varying stiffness and time-varying error. The system is in a meshing state when $x \in S_1$; the system is in an impact state when $x \in S_1$ and $x \in S_2$ simultaneously. Because of the existence of the backlash, the system will undergo different states. When the system makes the transition from the meshing state to the impact state, the solution trajectory of the system will cross the boundary $K(x) = 0$ and the motion state of the system will change, which may result in the state instability. Therefore, we will analyze the local behaviors of the system in the vicinity of the boundary.

3. Grazing bifurcation mechanism

In the process of transmission, on the moment that the backlash appears immediately, the solution trajectory of the system which is in the meshing state will hit the boundary tangentially without crossing it, which is defined as the grazing state. If a small perturbation caused by a system parameter is applied to the system, the backlash will appear between the meshing gears, which will result in the change of the dynamical behaviors of the system. The evolution of the grazing trajectory is shown in Fig. 3.

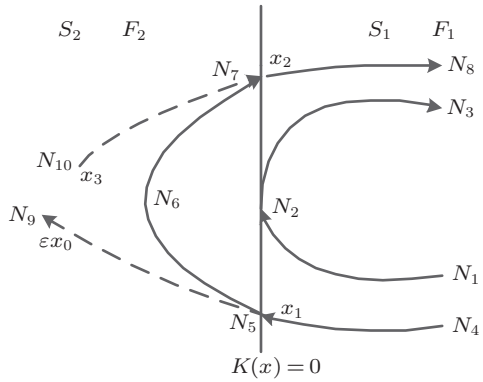


Fig. 3. The schematic diagram of zero-time discontinuous mapping (ZDM).

The solution trajectory $N_1 \to N_2 \to N_3$ is the grazing trajectory. When influenced by a small perturbation caused by a system parameter, the grazing trajectory will cross the boundary and evolve into another trajectory $N_4 \to N_5 \to N_6 \to N_7 \to N_8$. $N_4 \to N_5$ and $N_7 \to N_8$ are the segments of the trajectory controlled by the vector field F_1 in the state space S_1; $N_5 \to N_6 \to N_7$ is the segment of the trajectory controlled by the vector field F_2 in the state space S_2; $N_5 \to N_9$ and $N_{10} \to N_7$ are the segments of the virtual trajectories controlled by the vector field F_1 when the boundary is ingnored. The zero-time discontinuous mapping (ZDM) is introduced to describe the influence of the vector field F_2 on the dynamical behaviors of the system when the solution trajectory is crossing the boundary.

In order to compute the trajectory $N_4 \to N_5 \to N_6 \to N_7 \to N_8$, the first segment ($N_4 \to N_5 \to N_9$) can be computed using the vector field F_1, even if it crosses the boundary. Then, the ZDM (i.e., $N_9 \to N_{10}$) can be applied to take into account the fact that the system has crossed the boundary. Finally, the second segment ($N_{10} \to N_7 \to N_8$) can be computed using the vector field F_1 again.

On the basis of this, choosing a fixed phase plane as the Poincare section, the Poincare mapping of the relative rotation system (18) with a backlash non-smooth characteristic under the oil film force is deduced by combining the ZDM. The Jacobian matrix of the Poincare mapping can be obtained when the ZDM is used as a special impact mapping. Then, the Floquet theory is applied to analyze the grazing bifurcation mechanism of the system.

3.1. The grazing conditions

When $P_m > P_q$, at $x = (0,0,0)^T$, the system (18) satisfies the following grazing conditions:[37]

$$K(x^*) = 0, \tag{19}$$

$$\left.\frac{\partial K}{\partial x}\right|_{x^*} \neq 0, \tag{20}$$

$$\left.\frac{\partial K}{\partial x}\right|_{x^*} F_1(x^*) = 0, \tag{21}$$

$$\left[\left(\frac{\partial^2 K}{\partial x^2}F_1\right)F_1 + \frac{\partial K}{\partial x}\left(\frac{\partial F_1}{\partial x}F_1\right)\right]\Bigg|_{x^*} > 0. \tag{22}$$

Thus, the grazing point is $x^* = (0,0,0)^T$, denoted by O. The ZDM is introduced to describe the influence of the vector field F_2 on the dynamical behaviors of the system (18) when the solution trajectory is crossing the boundary.

3.2. The zero-time discontinuous mapping

The flows $\Phi_i(x,t)$, $i = 1,2$ (i.e., the solution trajectories of the system) which are generated by the vector fields F_i ($i = 1,2$) of the system (18) can be defined as the quantities that satisfy

$$\frac{\partial}{\partial t}\Phi_i(x,t) = F_i(\Phi_i(x,t)), \quad \Phi_i(x,0) = x. \tag{23}$$

Now, because of the smoothness of the vector fields F_i ($i = 1,2$), each of the system flows $\Phi_i(x,t)$, $i = 1,2$ can be expanded as a Taylor series about the grazing point as

$$\Phi_i(x,t)$$

$$
\begin{aligned}
&= \Phi_i + \frac{\partial \Phi_i}{\partial x}x + \frac{\partial \Phi_i}{\partial t}t + \frac{1}{2}\frac{\partial^2 \Phi_i}{\partial t^2}t^2 + \frac{\partial^2 \Phi_i}{\partial x \partial t}xt \\
&\quad + \frac{1}{6}\left(\frac{\partial^3 \Phi_i}{\partial x^3}x^3 + \frac{\partial^3 \Phi_i}{\partial t^3}t^3 + 3\frac{\partial^3 \Phi_i}{\partial x \partial t^2}xt^2 + 3\frac{\partial^3 \Phi_i}{\partial x^2 \partial t}x^2 t\right) \\
&\quad + \frac{1}{24}\left(\frac{\partial^4 \Phi_i}{\partial x^4}x^4 + \frac{\partial^4 \Phi_i}{\partial t^4}t^4 + 4\frac{\partial^4 \Phi_i}{\partial x^3 \partial t}x^3 t\right. \\
&\quad \left. + 6\frac{\partial^4 \Phi_i}{\partial x^2 \partial t^2}x^2 t^2 + 4\frac{\partial^4 \Phi_i}{\partial x \partial t^3}xt^3\right). \qquad (24)
\end{aligned}
$$

Note that a shorthand notation has been used here for the higher-order derivative terms, for example

$$
\frac{\partial^3 \Phi}{\partial x^3}x^3 = \sum_{i,j,k=1,2,3} \frac{\partial^3 \Phi}{\partial x_i x_j x_k}x_i x_j x_k.
$$

Using the expression in Eq. (23) and the fact that

$$
\frac{\partial^2 \Phi_i}{\partial t^2} = \frac{\partial F_i}{\partial t} = \frac{\partial F_i}{\partial \Phi_i}\frac{\partial \Phi_i}{\partial t} = \frac{\partial F_i}{\partial x}F_i,
$$

We can obtain from Eq. (24) that

$$
\begin{aligned}
\Phi_i(x,t) &= x + F_i t + \frac{1}{2}\frac{\partial F_i}{\partial x}F_i t^2 + \frac{\partial F_i}{\partial x}xt \\
&\quad + \frac{1}{6}\left(\frac{\partial^2 F_i}{\partial x^2}F_i^2 + \left(\frac{\partial F_i}{\partial x}\right)^2 F_i\right)t^3 \\
&\quad + \frac{1}{2}\frac{\partial^2 F_i}{\partial x^2}x^2 t + \frac{1}{2}\left(\frac{\partial^2 F_i}{\partial x^2}F_i + \left(\frac{\partial F_i}{\partial x}\right)^2\right)xt^2 \\
&\quad + \frac{1}{24}\left[\frac{\partial^3 F_i}{\partial x^3}F_i^3 + \frac{\partial^2 F_i}{\partial x^2}\left(F_i\frac{\partial F_i}{\partial x} + \frac{\partial F_i}{\partial x}F_i\right)\right. \\
&\quad \left. + \left(\frac{\partial^2 F_i}{\partial x^2}\frac{\partial F_i}{\partial x} + \frac{\partial F_i}{\partial x}\frac{\partial^2 F_i}{\partial x^2}\right)F_i + (\frac{\partial F_i}{\partial x})^3 F_i\right]t^4 \\
&\quad + \frac{1}{6}\frac{\partial^3 F_i}{\partial x^3}x^3 t + \frac{1}{4}\left(\frac{\partial^3 F_i}{\partial x^3}F_i + \frac{\partial F_i}{\partial x}\frac{\partial^2 F_i}{\partial x^2}\right)x^2 t^2 \\
&\quad + \frac{1}{6}\left[\frac{\partial^3 F_i}{\partial x^3}F_i^2 + \frac{\partial^2 F_i}{\partial x^2}\frac{\partial F_i}{\partial x}F_i + \frac{\partial^2 F_i}{\partial x^2}F_i\frac{\partial F_i}{\partial x}\right. \\
&\quad \left. + \left(\frac{\partial^2 F_i}{\partial x^2}F_i\frac{\partial F_i}{\partial x} + \frac{\partial F_i}{\partial x}\frac{\partial^2 F_i}{\partial x^2}F_i\right) + \left(\frac{\partial F_i}{\partial x}\right)^3\right]xt^3 \\
&:= x + F_i t + a_i t^2 + b_i xt + c_i t^3 + d_i x^2 t \\
&\quad + e_i xt^2 + f_i t^4 + g_i x^3 t + h_i x^2 t^2 + j_i xt^3 + O(5). \qquad (25)
\end{aligned}
$$

As shown in Fig. 3, the ZDM $\varepsilon x_0 \to x_3$ is split into three pieces. Assuming that the time from εx_0 to x_1 is $-\delta$, the Taylor expansion of x_1 about the grazing point becomes

$$
\begin{aligned}
x_1 &= \Phi_1(\varepsilon x_0, -\delta) \\
&= \varepsilon x_0 - \delta F_1 + \delta^2 a_1 - \varepsilon\delta b_1 x_0 - \delta^3 c_1 \\
&\quad - \varepsilon^2\delta d_1 x_0^2 + \varepsilon\delta^2 e_1 x_0 + \delta^4 f_1 - \varepsilon^3\delta g_1 x_0^3 \\
&\quad + \varepsilon^2\delta^2 h_1 x_0^2 - \varepsilon\delta^3 j_1 x_0 + O(5). \qquad (26)
\end{aligned}
$$

At point x_1, which is in the boundary, $K(x_1) = 0$, so

$$
K(x_1) = K(0) + \langle \nabla K, x_1 \rangle = \langle \nabla K, x_1 \rangle = 0. \qquad (27)
$$

By substituting the Taylor expansion of Eq. (26) into Eq. (27), the result is

$$
\delta = \gamma_1 \varepsilon^{1/2} + \gamma_2 \varepsilon + \gamma_3 \varepsilon^{3/2} + O(\varepsilon^2), \qquad (28)
$$

where

$$
\begin{aligned}
\gamma_1 &= \sqrt{\frac{\langle \nabla K, x_0 \rangle}{\langle \nabla K, a_1 \rangle}}, \\
\gamma_2 &= \frac{\langle \nabla K, b_1 x_0 \rangle + \langle \nabla K, c_1 \gamma_1^2 \rangle}{2\langle \nabla K, a_1 \rangle}, \\
\gamma_3 &= -\frac{\langle \nabla K, a_1\gamma_2^2 \rangle + \langle \nabla K, e_1 x_0 \gamma_1^2 \rangle - \langle \nabla K, b_1 x_0 \gamma_2 \rangle - 3\langle \nabla K, c_1 \gamma_1^2 \gamma_2 \rangle}{2\langle \nabla K, a_1 \gamma_1 \rangle} - \frac{\langle \nabla K, f_1 \gamma_1^4 \rangle}{2\langle \nabla K, a_1 \gamma_1 \rangle},
\end{aligned}
$$

$$
x_1 = \chi_1 \varepsilon^{1/2} + \chi_2 \varepsilon + \chi_3 \varepsilon^{3/2} + O(\varepsilon^2), \qquad (29)
$$

where

$$
\begin{aligned}
&\chi_1 = -F_1\gamma_1, \quad \chi_2 = x_0 - \gamma_2 F_1 + a_1\gamma_1^2, \\
&\chi_3 = -b_1 x_0 \gamma_1 + 2a_1\gamma_1\gamma_2 - \gamma_3 F_1 - c_1\gamma_1^3.
\end{aligned}
$$

Assuming that the time from x_1 to x_2 is Δ, following the same procedure as before, it is found that

$$
\begin{aligned}
x_2 &= \Phi_2(x_1, \Delta) = x_1 + \Delta F_2 + \Delta^2 a_2 + \Delta b_2 x_1 \\
&\quad + \Delta^3 c_2 + \Delta d_2 x_1^2 + \Delta^2 e_2 x_1 + \Delta^4 f_2 \\
&\quad + \Delta g_2 x_1^3 + \Delta^2 h_2 x_1^2 + \Delta^3 j_2 x_1 + O(5), \qquad (30)
\end{aligned}
$$

$$
\langle \nabla K, x_2 \rangle = 0. \qquad (31)
$$

Hence, it follows that

$$
\Delta = \nu_1 \varepsilon^{1/2} + \nu_2 \varepsilon + \nu_3 \varepsilon^{3/2} + O(\varepsilon^2), \qquad (32)
$$

where

$$
\begin{aligned}
\nu_1 &= \frac{\langle \nabla K, b_2 F_1 \rangle \gamma_1}{\langle \nabla K, a_2 \rangle}, \\
\nu_2 &= -\frac{\nu_1\left[\langle \nabla K, d_2\chi_1^2 \rangle + \langle \nabla K, c_2\nu_1^2 \rangle + \langle \nabla K, b_2\chi_2 \rangle + \langle \nabla K, e_2\chi_1\nu_1 \rangle\right]}{2\langle \nabla K, a_2\nu_1 \rangle + \langle \nabla K, b_2\chi_1 \rangle}, \\
\nu_3 &= -\frac{\langle \nabla K, j_2\chi_1\nu_1^3 \rangle + \langle \nabla K, b_2\chi_3\nu_1 \rangle + \langle \nabla K, a_2\nu_2^2 \rangle + 2\langle \nabla K, d_2\chi_1\chi_2\nu_1 \rangle}{2\langle \nabla K, a_2\nu_1 \rangle + \langle \nabla K, b_2\chi_1 \rangle}
\end{aligned}
$$

$$+\frac{-\langle\nabla K,b_2\chi_2\nu_2\rangle-\langle\nabla K,b_2\chi_2\nu_2\rangle-\langle\nabla K,f_2\nu_1^4\rangle+2\langle\nabla K,e_2\chi_1\nu_1\nu_2\rangle}{2\langle\nabla K,a_2\nu_1\rangle+\langle\nabla K,b_2\chi_1\rangle}$$
$$+\frac{3\langle\nabla K,c_2\nu_1^2\nu_2\rangle+\langle\nabla K,e_2\chi_2\nu_1^2\rangle+\langle\nabla K,h_2\chi_1\nu_1^2\rangle+\langle\nabla K,d_2\chi_1^2\nu_2\rangle}{2\langle\nabla K,a_2\nu_1\rangle+\langle\nabla K,b_2\chi_1\rangle}+\frac{\langle\nabla K,g_2\chi_1^3\nu_1\rangle}{2\langle\nabla K,a_2\nu_1\rangle+\langle\nabla K,b_2\chi_1\rangle}.$$

Assuming that the time from x_2 to x_3 is $\delta-\Delta$, in order to ensure that the total time is zero for the mapping $\varepsilon x_0\to x_3$, then,

$$\begin{aligned}x_3 &= \Phi_1(x_2,\delta-\Delta)\\ &= x_2+(\delta-\Delta)F_1\\ &\quad+(\delta-\Delta)^2a_1+(\delta-\Delta)b_1x_2\\ &\quad+(\delta-\Delta)^3c_1+(\delta-\Delta)d_1x_2^2+(\delta-\Delta)^2e_1x_2\\ &\quad+(\delta-\Delta)^4f_1+(\delta-\Delta)g_1x_2^3\\ &\quad+(\delta-\Delta)^2h_1x_2^2+(\delta-\Delta)^3j_1x_2+O(5).\end{aligned}\tag{33}$$

The system (18) has a continuous form at the point of grazing discontinuity. At the grazing point, $F_1=F_2$. This condition gives rise to a 3/2 singularity in the ZDM. Due to the continuous nature of the vector fields at the grazing point, $O(\varepsilon^{1/2})$ terms go to zero, and $O(\varepsilon)$ coefficients become x_0. Further calculation of $O(\varepsilon^{3/2})$ terms yields the ZDM. Therefore, combining the actual formulas of F_1 and F_2 in system (18), the ZDM has a leading order term of the form

$$x_3=\varepsilon x_0+\frac{2}{3}\frac{(-2\varepsilon x_{10})^{3/2}}{(P_{\rm m}-P_{\rm q})^{1/2}(2\varsigma+\mu_{\rm o})}\begin{pmatrix}4\varsigma^2\\ \dfrac{-8\varsigma^3\mu_{\rm o}+4\sigma\varsigma^2+\sigma\mu_{\rm o}^2-4\varsigma\mu_{\rm o}-4\varsigma^2-\mu_{\rm o}^2+4\sigma\varsigma\mu_{\rm o}}{2\varsigma+\mu_{\rm o}}\\ 0\end{pmatrix},\tag{34}$$

which is the ZDM denoted by G. Next, the Poincare mapping will be deduced to analyze the local dynamic characteristics in the vicinity of the grazing point.

3.3. The Poincare mapping

In order to obtain the Poincare mapping in the vicinity of the grazing point, a fixed phase plane is chosen as the Poincare section

$$\Pi=\{(x_1,x_2,x_3)|x_3=\Omega t_0,\quad \mod(t-t_0,T)=0\},\tag{35}$$

where $T=2\pi/\Omega$.

When the solution trajectory of the system does not cross the boundary, the system is controlled by the vector field F_1 and the Poincare mapping is a smooth mapping

$$P=P_{\rm smooth}.\tag{36}$$

The $P_{\rm smooth}$ is defined as

$$\begin{aligned}&P_{\rm smooth}:\Pi_{t_0}\to\Pi_{t_0+T},\\ &x_0\to x_{0+T}=\Phi_1(x_0,t_0+T).\end{aligned}\tag{37}$$

When the solution trajectory of the system crosses the boundary, the system is controlled by the vector field F_1 and the vector field F_2, and the ZDM is introduced to describe the influence of the vector field F_2 and the boundary on the dynamical behaviors of the system, so the Poincare mapping is a nonsmooth composite mapping as

$$P=P_{\rm nonsmooth}.\tag{38}$$

The $P_{\rm nonsmooth}$ is divided into three local mappings

$$P_1:\Pi_{t_0}\to\Pi_{t_-},\ \ x_0\to x_-=\Phi_1(x_0,t_*-t_0),\tag{39}$$
$$P_2:\Pi_{t_-}\to\Pi_{t_+},\ \ x_-\to x_+=G(x_-),\tag{40}$$
$$P_3:\Pi_{t_+}\to\Pi_{t_{0+T}},\ \ x_+\to x_{0+T}=\Phi_1(x_+,t_0+T-t_*).\tag{41}$$

Then, the Poincare mapping is

$$P=P_3\circ P_2\circ P_1,\tag{42}$$

where $P_3\circ P_2\circ P_1$ represents $P_3(P_2(P_1))$, i.e., $x_{0+T}=P(x_0)=P_3(P_2(P_1(x_0)))$.

The Poincare mapping can describe the change of the dynamical behaviors of the system in the vicinity of the grazing point.

3.4. Grazing bifurcation analysis

The change of the largest eigenvalue of the Jacobian matrix in the Poincare mapping can be used to analyze the change of the dynamical behaviors of system (18).

The ZDM which is a discrete mapping, just like the impact mapping, is regarded as a special impact mapping in this paper. Therefore, the Jacobian matrix of the Poincare mapping can be obtained by applying the impact theory.

When the solution trajectory of the system does not cross the boundary, the Jacobian matrix of the Poincare mapping which is a smooth mapping can be obtained by integrating Eqs. (43) and (44) from t_0 to t_0+T

$$\begin{cases}\dfrac{{\rm d}J}{{\rm d}t}=\dfrac{\partial F_1}{\partial x}J,\\ J(t=t_0)=I_3,\end{cases}\tag{43}$$

where I_3 is a 3×3 unit matrix, J is the Jacobian matrix at a certain moment, and F_1 is the vector field of system (18)

$$\begin{cases} \dfrac{\mathrm{d}x}{\mathrm{d}t} = F_1(x), \\ x(t=t_0) = x_0, \end{cases} \tag{44}$$

where x_0 is the initial value.

The Jacobian matrix of the Poincare mapping is

$$DP = J(t = t_0 + T). \tag{45}$$

When the solution trajectory of the system crosses the boundary, the Jacobian matrix of the Poincare mapping which is a nonsmooth composite mapping can be expressed as

$$DP = DP_3 \circ DP_2 \circ DP_1. \tag{46}$$

Here, P_1 and P_3 are both smooth mappings. Thus, DP_1 can be obtained by integrating Eqs. (43) and (44) from t_0 to t_*; DP_3 can be obtained by integrating Eqs. (43) and (44) from t_* to $t_0 + T - t_*$.

According to the impact theory, DP_2 is given by[34]

$$\begin{aligned} DP_2 = {} & [G_x(I - F_1K_x/(K_xF_1)) \\ & + F_1(G(x))K_x/(K_xF_1)]\big|_{x=x_-}, \end{aligned}$$

where $G_x = \partial G/\partial x$, $K_x = \partial K/\partial x$.

In conclusion, the Jacobian matrix of the Poincare mapping in the vicinity of the grazing point can be expressed as

$$DP = \begin{cases} J(t = t_0 + T), & \text{if the trajectory does not cross the boundary,} \\ DP_3 \circ DP_2 \circ DP_1, & \text{if the trajectory crosses the boundary.} \end{cases} \tag{47}$$

The change of the largest eigenvalue of the Jacobian matrix (47) can be used to analyze the grazing bifurcation mechanism of the system (18). The results are obtained according to the above analysis and the Floquet theory:

Theorem 1 If all the eigenvalues of the matrix DP in Eq. (47) are within the unit circle, the system is stable. Otherwise, the system will lose its stability. With the decrease of P_m, the grazing bifurcation will occur when the largest eigenvalue jumps out of the unit circle.

4. Numerical simulations

The external excitation influenced by the torque ripple or exterior factors is chosen as the bifurcation parameter to study the system. The system parameters are chosen as $\varsigma = 0.04$, $\sigma = 0.1$, $P_\mathrm{q} = 0.81$, $\Omega = 0.1$, $\eta = 1.2$, $c = 0.1207 \times 10^{-3}$. The change of the modulus of the largest eigenvalue of the Jacobian matrix (47) in the local area $0.8148 \le P_\mathrm{m} \le 0.8165$ is shown in Fig. 4.

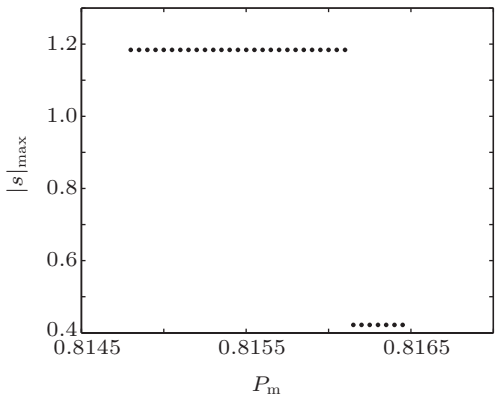


Fig. 4. The change diagram of the modulus of the largest eigenvalue.

As shown in Fig. 4, when $P_\mathrm{m} \ge 0.8162$, the modulus of the largest eigenvalue is less than 1, which means that all the eigenvalues are within the unit circle, so the system is stable; when $P_\mathrm{m} < 0.8162$, the modulus of the largest eigenvalue is greater than 1, which means that the largest eigenvalue jumps out of the unit circle, so the system becomes instable. The grazing bifurcation point is $P_\mathrm{m} = 0.8162$.

Next, the nonsmooth relative rotation system (18) will be analyzed to prove the validity of the conclusion. The bifurcation diagram of the system (18) is shown in Fig. 5.

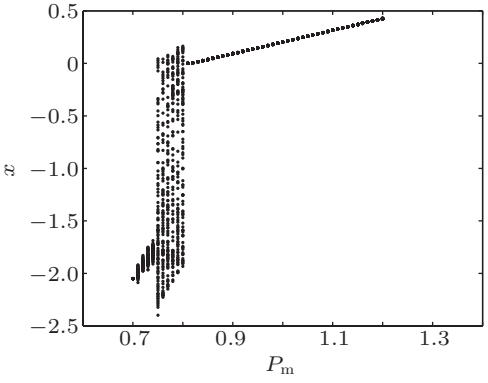


Fig. 5. The bifurcation diagram of system (18).

It can be seen from Fig. 5 that, with the decrease of P_m, the system in the single periodic stable motion undergoes the grazing motion and it later becomes chaotic motion because of the grazing bifurcation. When $P_\mathrm{m} > 0.82$, the system is in the single periodic stable motion. Meanwhile, the system is in the meshing state; when $P_\mathrm{m} < 0.82$, the system is in the chaotic motion. Meanwhile, the system is in the impact state. The grazing bifurcation point is $P_\mathrm{m} = 0.82$. The ZDM is the approximate calculation of the system, so there are some errors.

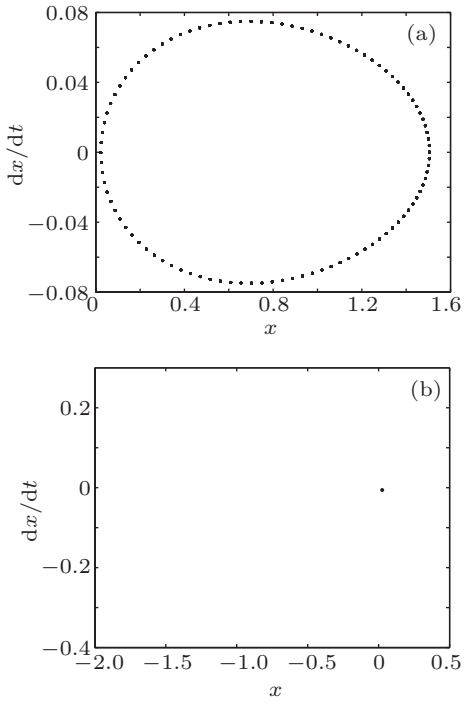


Fig. 6. The phase diagram and the Poincare section of $P_{\rm m} = 0.84$. (a) The phase diagram. (b) The Poincare section.

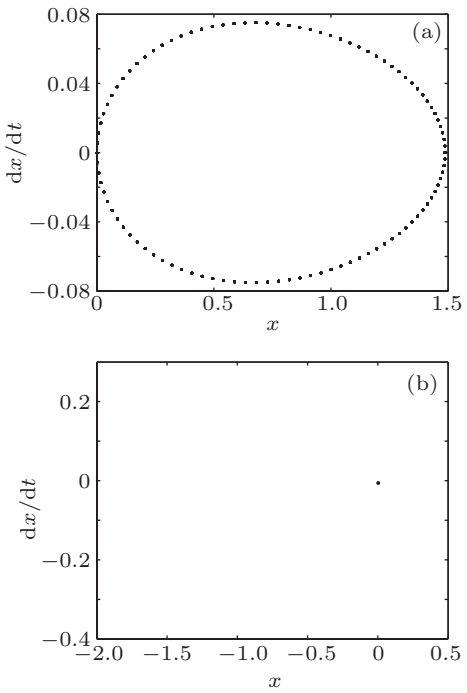


Fig. 7. The phase diagram and the Poincare section of $P_{\rm m} = 0.82$. (a) The phase diagram. (b) The Poincare section.

The phase diagrams and the Poincare sections with different values of $P_{\rm m}$ are shown in Figs. 6–8. As depicted in Figs. 6(a) and 6(b), when $P_{\rm m} = 0.84$, the system which has not undergone the grazing state is in the single periodic stable motion. Meanwhile, the system is in the meshing state. As shown in Figs. 7(a) and 7(b), when $P_{\rm m} = 0.82$, the system stays in the grazing state exactly, and its dynamical behavior has not changed, and the system is in the critical meshing state. When $P_{\rm m} = 0.80$, the system enters chaotic motion after the grazing state, and the system is in the impact state. The ruleless state shown in Fig. 8(a) and the obvious fractal structures shown in Fig. 8(b) can prove the existence of the chaotic motion.

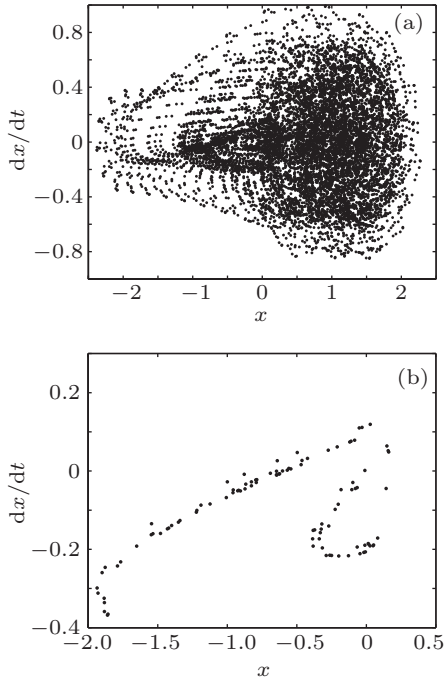


Fig. 8. The phase diagram and the Poincare section of $P_{\rm m} = 0.80$. (a) The phase diagram. (b) The Poincare section.

5. Conclusion

In this paper, considering the oil film, backlash, time-varying stiffness, and time-varying error, the dynamical equation of a relative rotation system with the backlash nonsmooth characteristic is deduced according to Newton's law. The grazing bifurcation mechanism of the system is analyzed as the external excitation changes. The research shows that with the decrease of the external excitation, the system transforms from the meshing state to the impact state. During this period, the grazing bifurcation occurs so that the dynamical behaviors of the system change from the single periodic stable motion to the chaos motion. Increasing the external excitation is propitious to suppressing the chaotic behaviors caused by the grazing bifurcation. These results have an important theoretical significance on reducing the vibration of the relative rotation systems with backlash. In addition, the research in our paper provides a reference for the further study of complex nonsmooth dynamic behaviors of large rotary machinery.

References

[1] Luo S K 1996 *J. Beijing Inst. Technol.* **16** 154 (in Chinese)
[2] Luo S K 1998 *Appl. Math. Mech.* **19** 45
[3] Luo S K, Fu J L and Chen X W 2001 *Acta Phys. Sin.* **50** 383 (in Chinese)

[4] Luo S K, Li Z J, Peng W and Li L 2013 *Acta Mech.* **224** 71
[5] Li Z J and Luo S K 2012 *Nonlinear Dyn.* **70** 1117
[6] Luo S K, Li Z J and Li L 2012 *Acta Mech.* **223** 2621
[7] Wang X Y and Wang M J 2008 *Physica A* **387** 3751
[8] Tang Y, Fang B, Zhang Y W and Li Q F 2011 *Journal of Vibration and Shock* **30** 269 (in Chinese)
[9] Ma C and Wang X Y 2012 *Commun. Nonlinear Sci. Numer. Simulat.* **17** 721
[10] Zhang L S, Cai L and Feng C W 2011 *Acta Electron. Sin.* **39** 5 (in Chinese)
[11] Wang X Y and Wang L L 2011 *Chin. Phys. B* **20** 050509
[12] Wu G and Cai L 2010 *Chin. J. Sci. Instrument* **31** 454 (in Chinese)
[13] Bao H M and Zhu Y S 2009 *Acta Electron. Sin.* **37** 1222 (in Chinese)
[14] Wang X Y, Liang Q Y and Meng J 2008 *Int. J. Mod. Phys. C* **19** 1389
[15] Wang X Y and Liang Q Y 2008 *Commun. Nonlinear Sci. Numer. Simulat.* **13** 913
[16] Chen J S, Zeng Y C, Chen S B and Li J B 2011 *Chin. J. Sci. Instrument* **32** 1710 (in Chinese)
[17] Liu B, Shi P M and Liu S 2009 *Acta Phys. Sin.* **58** 4383 (in Chinese)
[18] Liu B, Zhang Y K, Liu S and Wen Y 2010 *Acta Phys. Sin.* **59** 38 (in Chinese)
[19] Shi P M, Li J Z, Liu B and Han D Y 2011 *Acta Phys. Sin.* **60** 094501 (in Chinese)
[20] Meng Z, Fu L Y and Song M H 2013 *Acta Phys. Sin.* **62** 054501 (in Chinese)
[21] Li H B, Wang B H, Zhang Z Q, Liu S and Li Y S 2012 *Acta Phys. Sin.* **61** 094501 (in Chinese)
[22] Chen S Y and Tang J Y 2008 *J. Sound Vib.* **318** 1109
[23] Ma C and Wang X Y 2012 *Commun. Nonlinear Sci. Numer. Simulat.* **17** 721
[24] Lopez C, Malburet F and Barraco A 2012 *J. Comput. Nonlin. Dyn.* **7** 021014
[25] Xu L Z, Wang F and Hao X H 2012 *J. Comput. Nonlin. Dyn.* **8** 021016
[26] Luo A C J and Gegg B C 2006 *Commun. Nonlinear Sci. Numer. Simulat.* **11** 777
[27] Luo A C J and Gegg B C 2006 *J. Sound Vib.* **291** 132
[28] Luo A C J and Gegg B C 2006 *Int. J. Bifurcat. Chaos* **16** 3539
[29] Pavlovskaia E, Wiercigroch M and Banerjee S 2010 *Physica D* **239** 312
[30] Mason J F and Piiroinen P T 2011 *Chaos* **21** 013113
[31] Mason J F and Piiroinen P T 2012 *Chaos* **22** 013106
[32] Xu J, Li Q and Wang N 2011 *Appl. Math. Comput.* **217** 5537
[33] Humphries N and Piiroinen P T 2012 *Physica D* **241** 1911
[34] Hos C and Champneys A R 2012 *Physica D* **241** 2068
[35] Chavez J P and Wiercigroch M 2013 *Commun. Nonlinear Sci.* **18** 2571
[36] Wen S Z and Yang P R 1992 *Elasto Hydrodynamic Lubrication* (1st edn.) (Beijing: Tsinghua University Press) pp. 7–75
[37] Bernardo M D, Budd C F and Champneys A R 2001 *Physica D* **160** 222